Journal of Power Sources 218 (2012) 65–72

Contents lists available at SciVerse ScienceDirect

Journal of Power Sources

journal homepage: www.elsevier.com/locate/jpowsour

# Effect of microcracking on ionic conductivity in LATP

Spencer D. Jackman*, Raymond A. Cutler

*Department of Materials Science and Engineering, University of Utah, Salt Lake City, UT 84112, USA*

## HIGHLIGHTS

- Microcracking leads to high grain boundary impedance in LATP.
- Optimum total ionic conductivity of 0.7 mS $cm^{-1}$ and activation energy of ~0.35 eV.
- d.c. conductivity in aqueous LiOH measured as 1.6 mS $cm^{-1}$ at 50 °C.
- Biaxial membrane strength measured as 123 MPa with 1.1 MPa$\sqrt{m}$ fracture toughness.

## ARTICLE INFO

*Article history:*
Received 22 April 2012
Accepted 7 June 2012
Available online 28 June 2012

*Keywords:*
LATP
Ionic conductivity
Microcracking
Strength
Fracture toughness

## ABSTRACT

Because of high thermal expansion anisotropy, lithium aluminum titanium phosphate (LATP) is prone to microcrack generation. While much attention has been given to the role of grain boundary phases on the ionic conductivity of LATP, the effect of microcracking is also expected to lower conductivity.

While all LATP materials characterized had grains larger than the critical size for microcracking, fine-grained (1.7 ± 0.7 μm) $Li_{1.3}Al_{0.3}Ti_{1.7}(PO_4)_3$ had twice the ionic conductivity of the same purity of coarse-grained (4.8 ± 1.9 μm) LATP at 323 K due to less extensive cracking at grain boundaries. While the increase in Young's modulus (81–115 GPa) and biaxial strength (26 ± 2 MPa to 123 ± 17 MPa) is consistent with the reduction in grain size, the increase in conductivity is a strong driving force for avoiding large LATP grains. Lower purity degraded ionic conductivity for similar grain sizes, as expected.

Single-edged precracked beam fracture toughness measurements showed that the fine-grained, high-purity LATP has a $K_{Ic}$ value of 1.1 ± 0.3 MPa$\sqrt{m}$. Flexural strength measurements (147 ± 14 MPa) indicated that the critical flaw size was on the order of 30 μm, with processing flaws still limiting strength. It is expected that as grain size is further reduced, strength and ionic conductivity will continue to improve in tandem until microcracking is eliminated.



## 1. Introduction

Consumer electronics, such as laptop computers and smart phones, drive current interest in and demand for lightweight, low-impedance Li-ion batteries. Liquid electrolyte-based systems with Li inorganic oxides as intercalation compounds [1,2] and polymer membrane separators dominate the commercialized Li-ion technology currently in use. While these systems have enjoyed much success and continue to do so, the possible use of Li-ion batteries in larger scale automotive and aerospace applications is accompanied by the necessity of higher capacity and energy storage with less loss of charge when not in use. Solid electrolytes with high potential and capacity could find use in such applications.

Hagman and Kierkegaard [3] reported fast transport of $Na^+$ ions through the sodium zirconium phosphate (NZP) structure ($Na_{1+x}Zr_2P_{3-x}Si_xO_{12}$). Hong et al. [4,5] and Goodenough et al. [6,7] pioneered the NZP family as fast ion conductors, realizing that $Li^+$ could be substituted for $Na^+$ in the structure. It is not only possible to replace $Na^+$ by $Li^+$, but $Ti^{4+}$ substitution for $Zr^{4+}$ results in LTP ($LiTi_2P_{3-x}Si_xO_{12}$) materials, which are called by the acronym LATP when $Al^{3+}$ is incorporated into the structure increasing the $Li^+$ concentration for charge neutrality [8]. The major advantage of LATP is high ionic conductivity near room temperature [9].

High thermal expansion anisotropy between the *a* and *c* lattice parameters is well documented in the NZP family of materials [10]. If grains exceed a critical size in polycrystalline materials, microcracking along grain boundaries occurs due to the difference in contraction upon cooling from the sintering temperature.

* Corresponding author. Tel.: +1 801 581 6863; fax: +1 801 581 4816.
*E-mail address:* spencerdjackman@gmail.com (S.D. Jackman).

0378-7753/$ – see front matter © 2012 Elsevier B.V. All rights reserved.
http://dx.doi.org/10.1016/j.jpowsour.2012.06.081

Cleveland and Bradt [11,12] showed that critical grain size for microcracking, $GS_{critical}$, could be calculated as

$$GS_{critical} = \frac{14.4\gamma_f}{E(\Delta\alpha_{max})^2(\Delta T)^2} \quad (1)$$

where $\gamma_f$ is the fracture surface energy for grain boundary microcracking, $\Delta\alpha_{max}$ is the difference between the maximum and minimum principal axial thermal expansion coefficients of the unit cell, $\Delta T$ is the temperature differential to initiate microcracking during cooling, and $E$ is Young's modulus. Bradt [12] showed that the critical grain size for NZP materials ranged between 2 and 13 μm. The higher anisotropy of LTP materials [13,14] suggests that the critical grain size for LATP may be below 2 μm.

Although the NZP structure is highly disordered, it exhibits open channels between ion sites, giving LATP materials relatively high ionic conduction through the lattice (bulk) of $10^{-3}$ S cm$^{-1}$ even at ambient temperature [8]. Impurities often segregate to grain boundaries and lower conductivity in ionic conductors. Coarser grained materials have fewer grain boundaries; therefore, as grain size decreases the grain boundary influence on conductivity increases, lowering the total conductivity [15]. In general, as grains become coarser, the bulk conductivity component of total ionic conductivity begins to dominate. In microcracked materials, however, one might expect that ionic conductivity would increase as grain size decreases, since microcracks will impede ionic conductivity.

The Hall–Petch relationship, which is often used to explain the effect of grain size on strength for metals, suggests that the strength of a material should increase with the inverse square root of grain size. Metals are strengthened by dislocation motion so that grains act as barriers for dislocation movement, increasing strength. In ceramics, dislocation mobility is low at ambient temperatures, so grain size is only a way to increase strength if it acts as the critical flaw or is linked to the critical flaw size. For many polycrystalline ceramics, processing allows the grain size to influence the critical flaw size such that strength increases as the grain size decreases [16]. A better predictor of strength is the critical flaw size, $c$, which is related to fracture strength, $\sigma_f$, as

$$K_{Ic} = Y\sigma_f\sqrt{c} \quad (2)$$

where $K_{Ic}$ is the fracture toughness and $Y$ is a geometrical factor dependent on both crack size and shape. The fracture toughness of LATP is expected to be low, since NZP has a fracture toughness of 1.0 ± 0.2 MPa√m [17]. Strength is expected to be related to the inverse square root of the critical flaw size, which may be a pore, network of microcracks, agglomeration of grains, or other defects introduced during processing.

The purpose of this paper is to show evidence that microcracking can lower the ionic conductivity of LATP materials, as well as determine the fracture toughness of fine-grained LATP so that the critical flaw size can be assessed. It was hypothesized that by lowering grain size, ionic conductivity and strength could be simultaneously increased for high-purity $Li_{1.3}Al_{0.3}Ti_{1.7}(PO_4)_3$.

## 2. Experimental

### 2.1. Phase purity and characterization of physical and mechanical properties

All testing was performed on sintered LATP specimens that were obtained from Ceramatec, Inc. (Salt Lake City, Utah). Four experimental grades were prepared using proprietary processing. These specimens were characterized using an X-ray diffractometer (Philips PW3040) to verify the LATP phase and identify any secondary phases. Scans were conducted with Cu $K_\alpha$ radiation over a $2\theta$ range of 15–75° using a step size of 0.02° and a 0.05 s dwell time. Rietveld refinement was used to quantify the amount of additional phases when present [18]. LATP specimens were categorized as either low-purity, fine-grained (LPFG), moderate-purity, fine-grained (MPFG), high-purity, coarse-grained (HPCG), or high-purity, fine-grained (HPFG) specimens based on experimental findings. LPFG and MPFG specimens were specimens with distinct secondary phases while HPCG and HPFG specimens were phase-pure by X-ray diffraction (XRD) with coarse-grained and fine-grained microstructures, respectively.

Densities based on Archimedes' principle were measured in water, from which the percentage of open porosity could also be calculated. The microstructure of those specimens used for strength and conductivity testing was examined using a scanning electron microscope (JEOL JSM-5900LV SEM) and a microhardness tester (LECO LM-100). Fracture surfaces of specimens broken during biaxial strength testing as well as surfaces polished with an automatic polisher (LECO Spectrum System 2000) were examined.

The biaxial strength of compositions with varying grain sizes and both phase-pure LATP and batches showing secondary phases were determined using a universal testing machine (Instron model 5566) with a 1 kN load cell using a ring-on-ring test (ASTM C1499-04). The support structure had a radius on the compressive side of 6.5 mm and a radius on the tension side of 9.5 mm. A thin piece of adhesive was placed on the compressive side to keep the broken disk pieces together. A steel ball was held with the top ring fixture through lowering until contact was made with the ceramic. The rate for the applied load was 0.5 mm min$^{-1}$, and data were collected every 50 ms. The biaxial fracture strength, $\sigma_b$, was calculated using [19]

$$\sigma_b = \frac{3P}{2\pi t^2}\left[(1-\nu)\frac{D_S - D_L}{2D^2} + (1+\nu)\ln\left(\frac{D_S}{D_L}\right)\right] \quad (3)$$

where $P$ is the applied load, $t$ is the specimen thickness, $\nu$ is Poisson's ratio, $D_S$ and $D_L$ are the support and load ring diameters, respectively, and $D$ is the specimen diameter. Biaxial strength measurements were important to shed light on the properties specific to LATP in the form of a thin, flat membrane. A Weibull probability function [20] is often used to characterize the reliability of brittle materials as

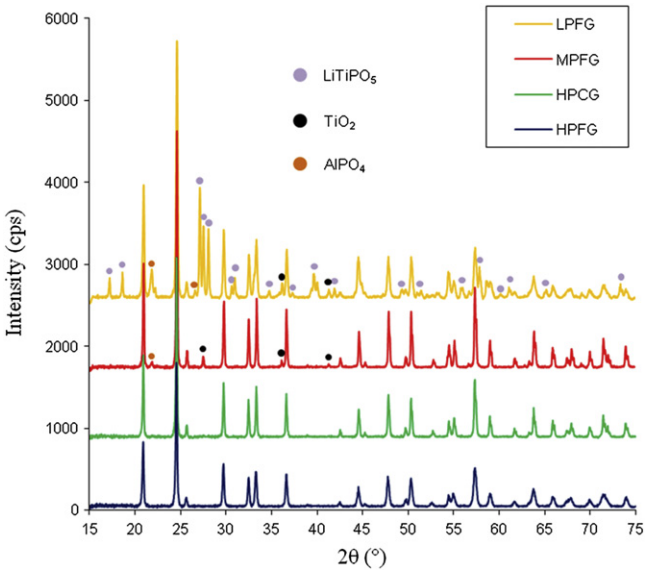


**Fig. 1.** XRD scans of LPFG, MPFG, HPCG, and HPFG LATP.

**Table 1**
Lattice parameters and unit cell volumes for LATP.

| | $a$ (Å) | $c$ (Å) | $\alpha$ (°) | $\gamma$ (°) | $V$ (Å$^3$) |
|---|---|---|---|---|---|
| HPCG | 8.507(1) | 20.821(2) | 90 | 120 | 1305.04 |
| HPFG | 8.482(2) | 20.804(5) | 90 | 120 | 1296.36 |
| Indexed values[a] | 8.513 | 20.878 | 90 | 120 | 1310.31 |

[a] Values correspond to LTP structure.

$$\ln\left(\ln\left(\frac{1}{1-F}\right)\right) = m\ln(\sigma_b) - m\ln(\sigma_0) \quad (4)$$

where $F$ is the probability of failure, $m$ is the Weibull modulus, and $\sigma_0$ is the characteristic strength. The Weibull modulus indicates the variability in measured strength, with a higher modulus correlating to greater consistency in strength. The characteristic stress is found when $\sigma_f$ is equal to $\sigma_0$, leading to an $F$ of 0.632, meaning there is a probability that 63.2% of specimens would fail at this calculated stress.

Flexural strength on bars of nominal dimensions 3 mm × 4 mm × 45 mm tested at a loading rate of 0.5 mm min$^{-1}$ was calculated as [21]

$$\sigma_f = \frac{1.5PS}{wt^2} \quad (5)$$

where $S$ is the difference between the inner and outer spans of the fixture (20 mm), $w$ is the specimen width and $t$ is the thickness.

Young's modulus measurements were taken at low strains on coarse and fine-gained specimens by using a strain gauge adhered to the test section of the specimen to determine the loading/unloading trends.

The single-edge precracked beam (SEPB) method (ASTM C1421-10) was used to measure fracture toughness. Bars were first indented with a diamond Knoop indenter at 98 N, and then precracked (Maruto model MBK-603C Precracker) with a 6 mm span. The fracture toughness was calculated as [22]

$$K_{Ic} = \frac{P(S_o - S_i)}{tw^{1.5}}\left(\frac{3\left(\frac{a}{w}\right)^{1.5}}{2\left(1-\frac{a}{w}\right)^{1.5}}\right)\left[1.9887 - 1.326\left(\frac{a}{w}\right) - \left(\frac{\left\{3.49 - 0.68\left(\frac{a}{w}\right) + 1.35\left(\frac{a}{w}\right)^2\right\}\left[\frac{a}{w}\right]\left\{1-\left(\frac{a}{w}\right)\right\}}{\left(1+\left(\frac{a}{w}\right)\right)^2}\right)\right] \quad (6)$$

where $S_i$ and $S_o$ are the inner and outer spans, respectively, and $a$ is the crack length. The value of $a/w$ was measured by analyzing the fracture surface with a stereomicroscope (Nikon SMZ1000) after the specimens had been tested.

Bars with nominal dimensions 5 mm × 5 mm × 15 mm were thermally cycled 3 times in a dilatometer (Unitherm Model 1161) between $T$ = 298 and 873 K with a heating and cooling rate of 2 K min$^{-1}$ to measure thermal expansion.

### 2.2. Ionic conductivity measurements

Pellets with a 15 mm diameter and 5 mm thickness were used for a.c. impedance measurements to provide enough resistance to

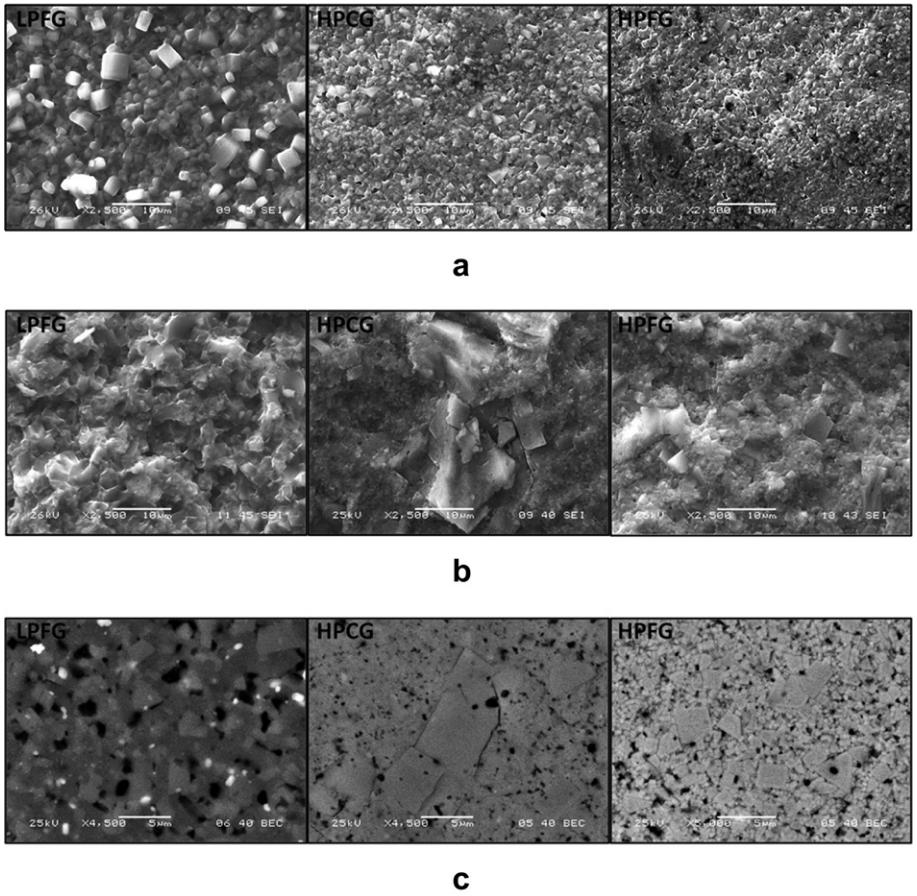


**Fig. 2.** SEM images of (a) as sintered surface, (b) fracture surface, and (c) polished surface of LPFG, HPCG, and HPFG LATP.

**Table 2**
Grain size and density of LATP.

| | Avg. grain size (μm) | Largest grains (μm) | Density (g cm$^{-3}$) | % Open porosity | % Theoretical density |
|---|---|---|---|---|---|
| LPFG | 2.2 ± 0.5 | 4 | 2.96 | 0.2 | NA |
| HPCG | 4.8 ± 1.9 | 30 | 2.86 | 1.5 | 97.0 |
| HPFG | 1.7 ± 0.7 | 9 | 2.82 | 0 | 95.6 |

ion transport at elevated temperatures that grain boundary arcs remained discernible from bulk arcs. Gold electrodes were sputtered onto both sides of the pellet with a sputter coater (Fullam EffaCoater). Five consecutive impedance measurements were taken at each temperature, ranging from ambient to 423 K in 25 K increments. Measurements were made with a spectrometer (Solartron SI 1260 Impedance/Gain-Phase) at an a.c. amplitude of 40 mV over a frequency range of 500 Hz to 10 MHz. The activation energy was obtained by plotting the logarithm of ionic conductivity times temperature as a function of inverse temperature based on the expected Arrhenius behavior.

For d.c. conductivity measurements, 25 mm diameter by 1 mm thick disks were used with Ni electrodes. Tests were conducted at $T = 323$ K with a current density of 25 mA cm$^{-2}$ in aqueous 7 wt% LiOH. Commercial software (*Labview*) was used to collect the voltage and current readings at 1 min intervals throughout the duration of the test. The voltage due to reactions at the electrodes was measured in situ without a membrane in the cell separating the cathode and anode compartments to obtain a 'blank' reading. This was used to calculate the resistance due solely to the membrane for d.c. conductivity calculations.

## 3. Results and discussion

### 3.1. Phase purity, physical and mechanical properties

Phase purity was evaluated by XRD with scans as displayed in Fig. 1. High-purity specimens were $Li_{1.3}Al_{0.3}Ti_{1.7}(PO_4)_3$ with no secondary phases detectable via XRD analysis. The low-purity specimens showed combinations of $AlPO_4$, $TiO_2$, and $LiTiPO_5$ phases that have low ionic conductivity and are frequently reported in the literature [23–25]. Rietveld refinement showed that LPFG specimens contained 36.5 wt.% $LiTiPO_5$ and 6.5 wt.% $AlPO_4$, the expected LATP phase comprising the remainder. MPFG specimens had less pronounced secondary phases, but 1.2 wt.% $AlPO_4$ and 4.0 wt.% $TiO_2$ were still detected by Rietveld analysis. Peaks corresponding to these phases are most prominent at $2\theta$ values of 21.8° ($AlPO_4$), 27.4° ($TiO_2$), 36.1° ($TiO_2$) and 41.2° ($TiO_2$). Kumar et al. [26] showed the deleterious effects of secondary phases on ionic conductivity at varying concentrations, sometimes lowering orders of magnitude over a few volume percents and eventually leading to space charge and blocking effects at higher concentrations. While the two high-purity materials may still have secondary phases below the detection limit of XRD, none were seen with either optical or SEM microscopy.

Calculated lattice parameters for both HPFG and HPCG samples are presented against indexed values in Table 1. The addition of Al into the lattice has the overall effect of shortening the unit cell dimensions, slightly decreasing the unit cell volume. This, however, does not appear to decrease the mobility of Li ions within the structure to any great extent [3]. Table 1 also presents evidence that there is no significant difference in lattice parameters between coarse and fine-grained materials tested in this study. The theoretical density, $\rho_{th}$, is easily calculated using the unit cell parameters as

$$\rho_{th} = \frac{Z \cdot MW}{V_c \cdot N_A} \quad (7)$$

where $Z$ is the number of molecules per unit cell, MW is molecular weight, $V_c$ is the volume of the unit cell, and $N_A$ is Avogadro's number. Using Equation (7), a theoretical density of 2.947 g cm$^{-3}$ was calculated for LATP, assuming a phase-pure material.

Fig. 2 shows a comparison of SEM images taken of as-sintered, fractured, and polished and etched surfaces for LPFG, HPCG, and HPFG specimens. Grain sizes calculated from the SEM images along with density data are summarized in Table 2. The images revealed porosity, in accord with expectation, based on density measurements. All materials have large grains which could lead to microcracking. The phase-pure materials had total porosity on the order of 3–5%. The open porosity in the coarse-grained material is evidence of macrocracking, due to the severe anisotropy in the LATP material, since all porosity is typically closed above about 93% of theoretical density.

While LPFG and HPFG specimens had comparable grain sizes, the LPFG image in Fig. 2(c) shows a more homogeneous size distribution. The secondary grain boundary phases present undoubtedly acted as a grain-growth inhibitor, and a more uniform fine-grained microstructure was maintained. HPCG and HPFG specimens both suffered from localized exaggerated grain growth, but HPCG displayed a much more dramatic effect. The large grains were easily observed both in the fractured and backscattered images, but fine grains surrounded these large grains in all images. Ostwald ripening appeared to be the key factor here, the coarse grains growing larger at the expense of the fine grains [27].

Comparisons of fracture surfaces illustrate that all specimens tested appear to have an intergranular mode of failure. Even a crack in a region of localized grain growth in an HPCG specimen seen in Fig. 3(a) did not appear to result in transgranular fracture, indicating that regardless of grain size, fracture was determined by a grain boundary phenomenon. It is hypothesized that as the grain size grows, microcracking dominates fracture behavior. Anisotropy in thermal expansion induces internal stresses that result in extensive microcracking due to high stresses and weak grain boundaries [28]. Fig. 3(b) provides evidence of this grain boundary macrocracking due to linked microcracks which greatly weaken the specimen and create a blockade for the ionic motion necessary for conductivity.

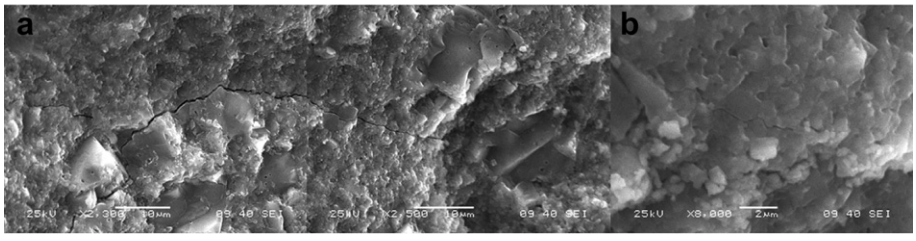


**Fig. 3.** SEM micrographs of (a) crack paths and (b) microcracks in an HPCG LATP.

The average grain sizes of HPCG and HPFG were 4.8 ± 1.9 μm and 1.7 ± 0.7 μm, respectively. Coarser particles used in processing often result in larger flaws than when finer particles are used. The difference in the biaxial strength between these two specimens is over 90 MPa (see Table 3), decreasing 79% from HPFG to HPCG specimens as shown in Fig. 4. This unusually large drop in strength over a less dramatic increase in grain size indicates there is more than just processing flaws which are influenced by grain size affecting the strength of the LATP specimens. A portion of the decreased strength can surely be attributed to larger defects manifest in coarser grains, but the largest contributing factor is believed to be increased microcracking. The low strength in the coarse grained material is a clear indication of severe microcracking. The higher Weibull modulus calculated for HPCG as compared to HPFG specimens can be explained by its decreased sensitivity to fabrication flaws. The critical flaws necessary to cause fracture at low stresses are inherent to the severely microcracked microstructure, and other flaws resulting from fabrication defects do not exhibit their influence on the mechanical strength.

The strength data and Young's modulus measurements are summarized in Table 3. Young's modulus measurements in HPFG over three successive runs showed no difference in measured modulus between runs, but hysteresis in the stress–strain behavior is confirmed in the slightly expanded view of Fig. 5. The strain behavior of the material as the grains are stretched apart under stress on the tensile side of the bar did not quite match with the behavior of the grains coming back together as this stress is released. This provides further evidence that microcracking exists in even the phase-pure specimens with the most homogeneous grain size measured in this study. The increase in Young's modulus from 81 GPa for HPCG to 115 GPa for HPFG specimens is the effect of decreased microcracking. The Young's modulus value of the extensively microcracked HPCG specimen is in the same range (65–85 GPa) as those previously reported on NZP materials [17,29]. Harshe et al. [30] measured Young's modulus as a function of temperature for a family of NZP materials, showing a maximum value of 105 GPa at high temperature (1373 K) when microcracks had healed. The value of 115 GPa for LATP appears to be a high modulus for a material from the NZP family. The flexural strength was slightly higher than the biaxial strength, which is not unusual for ceramic materials, where the volume of material under stress controls the strength. The Weibull modulus of 12 is a respectable value for a ceramic material. The fine-grained high-purity material appears to have acceptable strength for a membrane.

Only the fracture toughness of HPFG specimens was tested, the result being 1.1 ± 0.3 MPa√m, a value consistent with a previous measurement on NZP using the same technique [17]. Using Equation (2), the fracture toughness allows one to calculate the critical flaw size based on the mean flexural strength. Taking $Y = 1.29$, which is characteristic of surface flaws on flexural specimens, a critical flaw size of 31 μm was calculated for the HPFG LATP. This value is in agreement with the size of flaws identified at fracture origins as shown in Fig. 6. Higher strength is possible in these materials since it is clear that the critical flaw size is due to processing flaws and not large grains, consistent with expectations.

**Table 3**
Strength and Young's modulus of LATP.

| | Biaxial | | | Flexural | | |
|---|---|---|---|---|---|---|
| | $\sigma_{avg}$ (MPa) | $\sigma_0$ (MPa) | $m$ | $\sigma_{avg}$ (MPa) | $m$ | $E$ (GPa) |
| LPFG | 49 ± 12 | 54 | 5 | NA | NA | NA |
| HPCG | 26 ± 2 | 28 | 12 | NA | NA | 81 |
| HPFG | 123 ± 17 | 130 | 8 | 147 ± 14 | 12 | 115 |

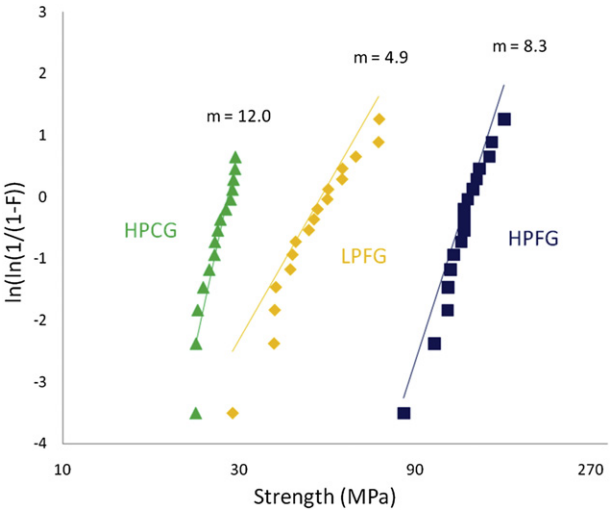


**Fig. 4.** Weibull plot of biaxial strength for LPFG, HPCG, and HPFG LATP.

Dilatometer results for HPCG and HPFG specimens are depicted in Fig. 7. The thermal expansion versus temperature graphs show distinct hysteresis in the path traced upon heating and cooling, although the effect is considerably more pronounced in the HPCG specimen. This suggests that although neither specimen was free from microcracking, the extent was greatly reduced in the HPFG specimen showing that reduced grain size lessened the tendency to microcrack, as was predicted.

Using Equation (1) to estimate the critical grain size for microcracking requires a value of the fracture surface energy for microcracking. Yamai and Oota [31] showed a linear relationship between the critical grain size for microcracking and $(\Delta\alpha_{max})^2$ for a family of NZP materials. Using their data, it is possible to calculate a value of 7 J m$^{-2}$ for $\gamma_f$, which is higher than might be expected based on single crystal data [32]. Using thermal expansion data at 1073 K given by Woodcock and Lightfoot [14], the Young's modulus value measured in this study, the estimated $GS_{critical}$ of LATP is 1.6 μm. If a more realistic value of 1 J m$^{-2}$ is taken for fracture energy [28], the critical grain size for microcracking decreases to 0.2 μm. Although these calculations are based on thermal expansion data for LTP and not LATP, data collected in this study for HPFG showed a linear thermal expansion of 11.2 × 10$^{-6}$ K$^{-1}$ at 873 K

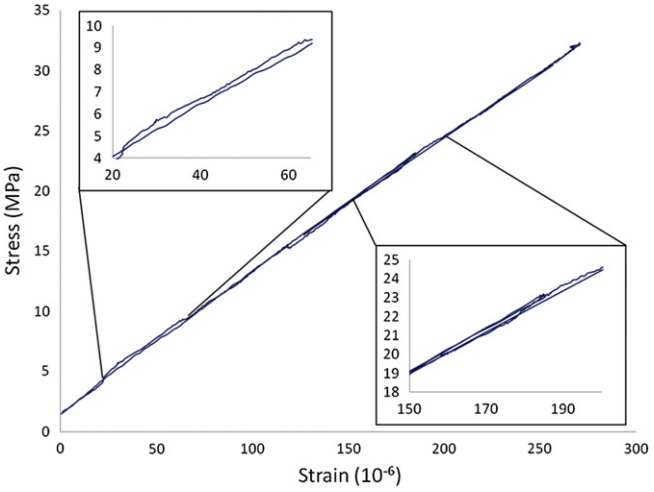


**Fig. 5.** Hysteresis in Young's modulus measurement of HPFG LATP.

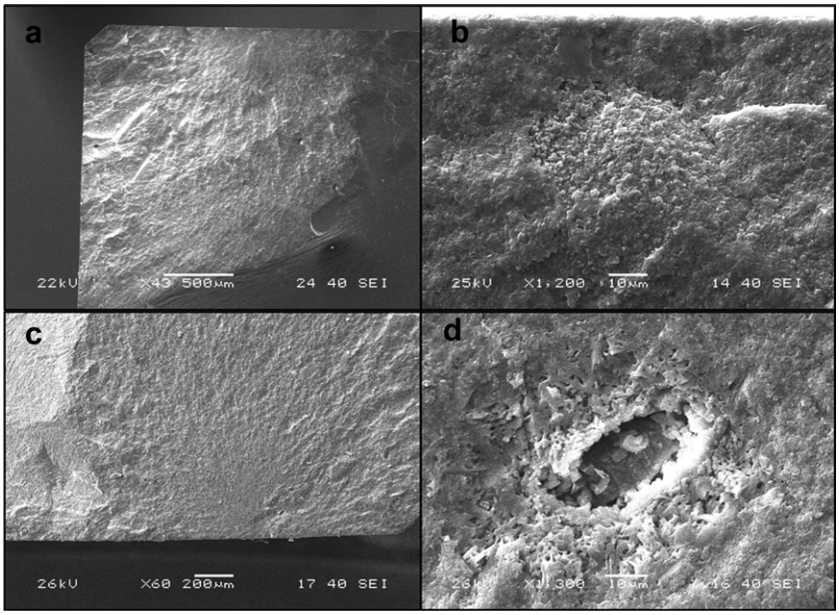


**Fig. 6.** SEM micrographs of (a,c) fracture zone and (b,d) higher magnification image of fracture origin in HPFG flexural strength bars.

which is in good agreement with that reported by Woodcock and Lightfoot of 11.5 $\times$ $10^{-6}$ $K^{-1}$ [14]. The trend that anisotropy increases with decreasing cation size shown by Huang [13] holds, making Li-ion based systems among the most susceptible to microcracking. This being the case, the microstructure images presented in this study give clear evidence that each tested specimen from all categories was surely microcracked to some extent.

The measured linear thermal expansion of the more severely microcracked HPCG (7.3 $\times$ $10^{-6}$ $K^{-1}$) is significantly lower than HPFG (11.2 $\times$ $10^{-6}$ $K^{-1}$). Since both specimens were confirmed to be of identical phase and composition, this discrepancy can be attributed to the increased presence of microcracked boundaries in HPCG, providing space for internal expansion to occur in the cracked spaces before causing bulk expansion [33].

### 3.2. Ionic conductivity

The most important characteristic of any solid electrolyte is its ability to conduct and transport ions. To some extent, no gain in mechanical properties can adequately compensate for a loss in ionic conductivity. Therefore, it is critical to ensure that the advantageous reduction in microcracks and improvements in strength and toughness correlate with maintaining and/or improving conductivity.

Fig. 8 gives the Nyquist plots of imaginary impedance versus real impedance for MPFG, HPCG, and HPFG materials. The difference in impedance at the grain boundary for each specimen can clearly be seen by the difference in size of the main semicircle (taken as the grain boundary arc based on capacitance) that eventually turns into a characteristic blocking electrode tail at low frequencies. The difference between high-purity samples is related to the microstructure, not the grain boundary chemistry. The limitations of the impedance spectrometer at frequencies above 10 MHz made full resolution of the bulk arc difficult, but it can be seen that all three semicircles converge to nearly the same nonzero value on the real impedance axis. The high frequency intercept of each trace was taken to be the bulk resistance for each specimen.

Fig. 9 is the Arrhenius plot of ionic conductivity and corresponding activation energies for tested specimens. The negative

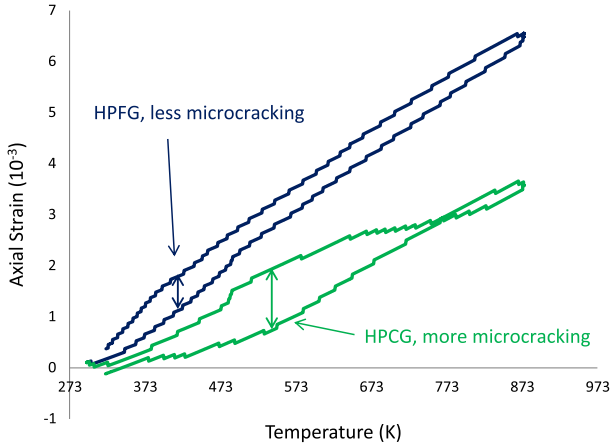


**Fig. 7.** Hysteresis in thermal expansion showing microcracking in both HPCG and HPFG LATP.

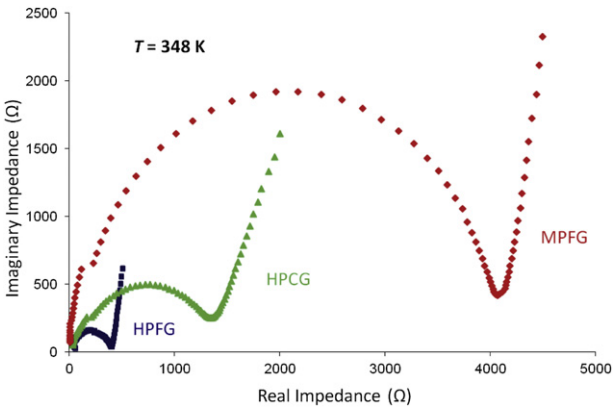


**Fig. 8.** Nyquist plots of imaginary versus real impedance for MPFG, HPCG, and HPFG LATP.

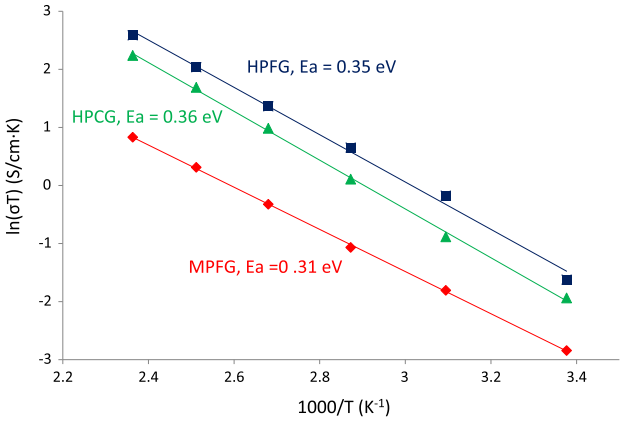


**Fig. 9.** Arrhenius plot of ionic conductivity for MPFG, HPCG, and HPFG LATP.

effects of high-impedance secondary phases (MPFG) and a decreased ability for ions to move at the grain boundaries due to microcracking (HPCG) are depicted. Conductivity data (bulk, grain boundary, and total) at all temperatures evaluated are given in Table 4. HPFG specimens had the highest conductivity at all temperatures, measuring 0.67 mS $cm^{-1}$ at room temperature, despite having a finer microstructure than HPCG. This counterintuitive trend of increasing grain boundary ionic conductivity with decreasing grain size is another indication of microcracking. It has been shown that for dense ceramic materials, grain boundary impedance is inversely related to grain size [34,35]. This trend is overshadowed, however, when ion movement is hindered by microcracks that are very large on the atomic scale, providing boundaries of void space through which ions cannot travel.

An effort was made by Leach to use impedance spectroscopy as a way of determining the onset and effect of microcracking during the tetragonal to monoclinic transformation in YSZ, but he was not able to measure the effect [36]. Microcracks on this scale (only visible with TEM) may not play a large role in ionic conductivity, but the present results with LATP indicate that when the extent of the cracking is measurable using strength, dilatometry, and modulus measurements, there is a pronounced increase in grain boundary impedance.

With the bulk conductivity being generally the same for all specimens and impedance at the grain boundary dominating the total conductivity, an increase in conductivity correlating with a decrease in grain size is likely explained by the reduction of grain boundary microcracks. It follows, then, that a dense sample free of microcracks would have the optimal ionic conductivity, with any further reduction in grain size resulting in an increase in grain boundary impedance.

The activation energy for all three materials was in the range of 0.31–0.36 eV, being on the lower end of the 0.3–0.5 eV range [37,38]. The 0.67 mS $cm^{-1}$ overall ambient temperature conductivity reported here is in excellent agreement with the 0.7 mS $cm^{-1}$ conductivity originally reported by Aono et al. in 1989 [8], but is higher than many recent reports and is coupled with an activation energy higher than the 0.2–0.3 eV range Aono measured. Thus conductivities at elevated temperatures were found to be higher than those previously reported.

Ionic conductivity measured via a.c. impedance, however, does not take into account all of the impedances introduced in most practical electrochemical cells, which require d.c. measurements to confirm the a.c. measurements. HPFG membranes were used in an aqueous testing cell to measure d.c. conductivity. The cell operated at an average voltage of 3.5 V and was stable enough to have confidence in the d.c. conductivity value measured to be 1.61 mS $cm^{-1}$. This is lower than the 2.60 mS $cm^{-1}$ total ionic conductivity at 323 K measured using the a.c. impedance method, but the 34% decrease is likely due to interfacial resistances in the system.

Several iterations of d.c. conductivity measurements showed that long-term testing of LATP materials in an aqueous LiOH environment was not possible due to rapid degradation of the membrane. The degradation appeared to be electrochemically driven, since under static conditions there did not appear to be any degradation. There is a need to determine the degradation mechanisms involved in aqueous environments for LATP.

## 4. Conclusions

While the single-most important factor in increasing the ionic conductivity in LATP-based solid electrolytes is clearly the elimination of high impedance secondary phases, which preferentially migrate to the grain boundaries, microcracking also lowers the conductivity of these materials when cracking is evident by Young's modulus measurements or using an SEM. Since the critical grain size for microcracking of $Li_{1.3}Al_{0.3}Ti_{1.7}(PO_4)_3$ is estimated to be less than or equal to 1.6 μm, very fine grains are required to avoid microcracked grain boundaries. None of the four experimental materials tested in this study satisfied this requirement when considering the largest grains in the microstructure. The bulk conductivity was virtually constant between LATP that was phase pure and LATP with secondary phases. The key to both improved strength and enhanced ionic conductivity in LATP materials will be processing a phase pure ceramic with all grains below the critical size for microcracking.

While none of the materials tested in this study had all grains at or below the critical size, the benefits of microcrack reduction were shown with thermal expansion, strength, and ionic conductivity measurements. The biaxial and flexural strengths measured were 123 ± 17 MPa and 147 ± 14 MPa, respectively, for phase-pure, high-purity, fine-grained LATP. While these strengths are still low for ionically conducting ceramics like cubic zirconia, they were more than double the strength of LATP with secondary phases. The bulk fracture toughness of LATP was measured to be 1.1 ± 0.3 MPa$\sqrt{m}$, which allowed the defect size to be determined. Defects were on the order of 30 μm for the best material and were not linked to

**Table 4**
Ionic conductivity of LATP from 298 to 423 K.

| $T$ (K) | $\sigma_b$ (mS $cm^{-1}$) | | | $\sigma_{gb}$ (mS $cm^{-1}$) | | | $\sigma_t$ (mS $cm^{-1}$) | | |
|---|---|---|---|---|---|---|---|---|---|
| | MPFG | HPCG | HPFG | MPFG | HPCG | HPFG | MPFG | HPCG | HPFG |
| 298 | 6.88 | 6.39 | 9.56 | 0.20 | 0.53 | 0.72 | 0.20 | 0.49 | 0.67 |
| 323 | 39.33 | 24.46 | 36.28 | 0.52 | 1.35 | 2.80 | 0.51 | 1.28 | 2.60 |
| 348 | 46.16 | 37.84 | 62.85 | 1.01 | 3.51 | 6.05 | 0.99 | 3.20 | 5.52 |
| 373 | 44.79 | 47.51 | 55.95 | 2.03 | 8.45 | 12.90 | 1.94 | 7.17 | 10.48 |
| 398 | 42.69 | 40.68 | 41.74 | 3.73 | 20.46 | 35.85 | 3.43 | 13.61 | 19.28 |
| 423 | 43.67 | 38.93 | 36.10 | 6.20 | 51.63 | 241.92 | 5.43 | 22.19 | 31.41 |

microcracks, suggesting that further improvements in strength are possible.

The most important result of this work is the clear evidence that microcracking led to decreased conductivity due to increased impedance at grain boundaries. While no transmission electron microscopy was performed to determine if grain boundaries were devoid of secondary phases, comparison of similar purity materials clearly showed conductivity increasing with decreasing grain size. Increases in both conductivity and strength appear to be possible for LATP by a further reduction in grain size. High-purity, fine-grained LATP had the highest total ionic conductivity at all temperatures, measuring 0.67 mS $cm^{-1}$ under ambient conditions with an activation energy of 0.35 eV. Improvements in grain boundary conductivity are not presumed to be an improvement in the actual conductivity of the material found at grain boundaries in LATP, but a reduction in void spaces through which Li ions cannot be conducted. Although the observation of lowered ionic conductivity due to microcracking is intuitive, it has never been shown that microcracking is a serious concern for the ionic conductivity of LATP ceramics. Microcracking should be avoided not only from a strength perspective, but from the standpoint of ionic conductivity.

## Acknowledgments

This work was performed at Ceramatec while Spencer Jackman was a CO-OP student and was partially funded by DOE grant DE-FE0000408. Technical discussions with Shekar Balagopal, Sai Bhavaraju, Tony Elangovan, Marc Flinders, John Gordon, Lyle Miller, and Mike Whittaker of Ceramatec were very helpful.

## References

[1] M.S. Whittingham, Science 192 (1976) 1126.
[2] B.C.H. Steele, Fast Ion Transp. Solids (1973) 103.
[3] L. Hagman, P. Kierkegaard, Acta Chem. Scand. 22 (1968) 1822.
[4] H.Y.P. Hong, Mater. Res. Bull. 11 (1976) 173.
[5] H.Y.P. Hong, J.A. Kafalas, M. Bayard, Mater. Res. Bull. 13 (1978) 757.
[6] J.B. Goodenough, H.Y.P. Hong, J.A. Kafalas, Mater. Res. Bull. 11 (1976) 203.
[7] J.B. Goodenough, Solid State Ionics 9/10 (1983) 793.
[8] H. Aono, E. Sugimoto, Y. Sadaoka, N. Imanaka, G. Adachi, J. Electrochem. Soc. 136 (1989) 590.
[9] J.W. Fergus, J. Power Sources 195 (2010) 4554.
[10] T. Oota, I. Yamai, J. Am. Ceram. Soc. 69 (1986) 1.
[11] J.J. Cleveland, R.C. Bradt, J. Am. Ceram. Soc. 61 (1978) 478.
[12] R.C. Bradt, Ceram. Trans. 52 (1995) 5.
[13] C.Y. Huang, D.K. Agrawal, H.A. McKinstry, J. Mater. Sci. 30 (1995) 3509.
[14] D.A. Woodcock, P. Lightfoot, J. Mater. Chem. 9 (1999) 2907.
[15] H.L. Tuller, Solid State Ionics 131 (2000) 143.
[16] J.P. Singh, A.V. Virkar, D.K. Shetty, R.S. Gordon, J. Am. Ceram. Soc. 62 (1979) 179.
[17] M.S. Sygnatowicz, Increasing the strength of NaSICON through improved processing, Senior thesis, University of Utah, 2007.
[18] H.M. Rietveld, J. Appl. Crystallogr. 2 (1988) 65.
[19] ASTMC1499-09, Standard Test Method for Monotonic Equibiaxial Flexure Strength of Advanced Ceramics at Ambient Temperature, ASTM, Philadelphia, PA, 2009.
[20] W. Weibull, J. Appl. Mech. Trans. ASME 18 (1951) 293.
[21] ASTM C1161-02c, Standard Test Method for Flexural Strength of Advanced Ceramics at Ambient Temperature, ASTM, Philadelphia, PA, 2008.
[22] ASTM 1421-10, Standard Method of Measuring Fracture Toughness of Advanced Ceramics at Ambient Temperature, ASTM, Philadelphia, PA, 2010.
[23] P.J. Gellings, H.J.M. Bouwmeester, CRC Handb. Solid State Electrochem., 1996, pp. 10.
[24] J. Kuwano, N. Sato, M. Kato, K. Takano, Solid State Ionics 70/71 (1994) 332.
[25] A.S. Best, K.M. Nairn, P.J. Newman, D.R. MacFarlane, M. Forsyth, M.J.G. Jak, J. Aust. Ceram. Soc. 34 (1998) 236.
[26] B. Kumar, S. Nellutla, J.S. Thokchom, C. Chen, J. Power Sources 160 (2006) 1329.
[27] P.W. Voorhees, J. Stat. Phys. (1985) 231.
[28] V. Tvergaard, J.W. Hutchinson, J. Am. Ceram. Soc. 71 (1988) 157.
[29] S. Limaye, R. Nageswaran, NZP Final Report for LoTEC, Inc., 1994.
[30] G. Harshe, D. Agrawal, S. Limaye, J. Am. Ceram. Soc. 77 (1994) 1965.
[31] I. Yamai, T. Oota, J. Am. Ceram. Soc. 76 (1993) 487.
[32] R.W. Rice, R.C. Pohanka, J. Am. Ceram. Soc. 62 (1979) 559.
[33] W.H. Rhodes, J. Am. Ceram. Soc. 64 (1981) 19.
[34] P. Mondal, A. Klein, W. Jaegermann, H. Hahn, Solid State Ionics 118 (1999) 331.
[35] M.K. Balapanov, R.A. Yakshibaev, I.B. Zinnurov, R.S. Musalimov, Bull. Russ. Acad. Sci. Phys. 70 (2006) 1064.
[36] C. Leach, J. Mater. Sci. Lett. 11 (1992) 306.
[37] P. Knauth, Solid State Ionics 180 (2009) 911.
[38] K. Arbi, J.M. Rojo, J. Sanz, J. Eur. Ceram. Soc. 27 (2007) 4215.